

Surveillance of Cis-Lunar Space via Space-based Sensor Network

Cesar G. Santoyo*

Georgia Institute of Technology, Atlanta, GA, 30318

Cis-lunar space remains an important habitat for the majority of spacecraft launched into orbit. As space launch services and missions evolved, the space domain was only destined to become more congested and logically complex. As a result, nations reacted to creating space monitoring systems such as the United States' Space Surveillance Network (SSN). Yet, efforts to fully surveil space activities, spacecraft life status and debris dangers have significant detection limitations for their respective optical and radar sensors. This begs the question: do in-space solutions exist for monitoring the near-Earth resident space object (RSO) population in cis-lunar space? This study will explore the feasibility of leveraging the Lagrangian points of the Earth-Moon system to create an in-space surveillance network that comprehensively fills the gaps in current optical and radar surveillance. Ultimately, this will result in a deeper understanding of any significant blind spots in the current ground-based SSN and the feasibility of an in-space surveillance network.

I. Introduction and Motivation

Nations derive their power from their ability to control strategic outcomes favorable to their interests [1, 2]. This concept of public policy has been applied to land, sea and air power for centuries making its relevance to the space domain of no surprise. Space endeavors have evolved from the pre-WWII Proto-Space Era, to Space 1.0, and most recently the Space 2.0 phase as characterized by Nicolas Peter of the European Space Agency (ESA) [2]. Arguably, space exploration has entered a new phase where low-cost launch services and space tourism companies begin to cement their presence in near-Earth orbits. Additionally, private-public partnerships (i.e. NASA, universities) in spacecraft development has contributed to growth in the number of spacecraft launches. The number of launched spacecraft grew from 5,000 in 2005 since Sputnik to the over 8,000 cataloged as launched in 2018 by the United Nations Office of State Affairs (UNOOSA) [3, 4]. The UNOOSA catalog quantity only considers structurally complete spacecraft or probes launched into orbit; this leaves ambiguity in the quantity of space debris born out of resident space object (RSO) collisions or catastrophic on-orbit events. The United States Strategic Command (USSTRATCOM) currently maintains the space catalog which has identified over 17,000 RSOs which includes small pieces of debris. The total number of RSOs in the USSTRATCOM's catalog is expected to increase with improved detection capabilities [3]. Additionally, the immensity of the growth and size of the launches is evident in the significant impact of the commercial space industry such as the \$168 billion of satellite industry revenues alone [5].

Currently, monitoring RSOs - which includes operational and defunct spacecraft as well as space debris - is done via the Space Surveillance Network (SSN) through a combination of both optical and radar sensors. The SSN is comprised of several categories of sensors: dedicated, collateral, and contributing sensors. Each of these observation sites provides a varying degree of commitment to the SSN. For the purposes of this study, only the dedicated sensors will be considered. Of course, this will limit the knowledge about observation deficiencies of the network but removes the ambiguity of time commitment to space surveillance from non-dedicated SSN sensors. For all observation sites, each surveillance commitment level has two types of sensors: optical and radar. This provides redundancies for both detection ranges and unfavorable observation conditions in which space objects can not be detected. However, radar has inherent limitations which restrict its ability to detect objects at distances greater than several thousand kilometers [3]. The average distance between the Earth and Moon is several hundreds of thousands of kilometers, making radar effective for only a fraction of the orbital volume. For nominal observation conditions (i.e. minimized Sun exposure, minimal cloud coverage)

*Graduate Research Assistant, School of Aerospace Engineering, Georgia Institute of Technology

electro-optical sensors such as GT-SORT - a Space Situational Awareness (SSA) research telescope - can be utilized when RSOs are beyond radar range [6]. Yet, there are cases where observation conditions are anomalous making optical observations difficult and uncertain[7]. These are scenarios such as when the alignment of the Sun's light, Moon and space region of interest create anomalous observation conditions. These limitations motivate exploring surveillance methods which are less susceptible to distance limitations and anomalous optical observation conditions.

Since the beginning of space exploration, cis-lunar space has remained a potential place where nation states will establish their power, where new conflicts will arise and where cutting-edge scientific inter-planetary missions would begin. Early on in the development of the space sector, Edson noted that space exploration was where the newest conflicts and opportunities will arise for humankind [8]. Cis-lunar space is formally defined as the region of space where the overwhelming majority of gravitational influence is due to the Earth-Moon System. Bobskill and Lupisella outline and analyze the potential of cis-lunar space for being the staging point for many deep-space missions as well as a home to a series of scientific endeavors such as automated rendezvous & docking, space robotics and crewed mission potential.[9]. Additionally, the work of Viscio et. al., as well as that of Martinez and Whitley provide a more in depth analysis of what technical requirements are needed for cis-lunar missions [10, 11]. Additionally, a couple of publications have been proposed for staging inter-planetary missions and space stations cis-lunar space [12, 13].

Within cis-lunar space, the Earth-Moon system contains 5 Lagrangian Points (L1 - L5) which provide unique opportunities for surveillance missions. For example, prior works have proposed utilizing L1 as a point for placing space stations or spacecraft. To thoroughly evaluate the feasibility of specific Lagrangian points, a stability analysis needs to be performed on a point by point basis. This is because some points are naturally more stable than others. With this in mind, the Lagrangian points can potentially be utilized as priority locations of interest for a space-based cis-lunar space surveillance system which complements the currently existing ground assets of the SSN. While the Lagrange points provide a unique opportunity, their location must be not only hypothetically feasible but practical with respect to current technological capabilities. This is an important limiting factor because a space-based surveillance network will require at least either optical or radar sensors.

Lagrange points are born out of the Restricted Three Body Problem and its special cases. If the system exists such that $m_3 \ll m_1, m_2$ and only a single spacecraft is being considered, and circular motion is assumed for the larger bodies, the Earth-Moon-Spacecraft system can be modeled as the Circular Restricted Three Body Problem (CRTBP). However, it is probable that more than a singular spacecraft is necessary to achieve comprehensive surveillance of cis-lunar space. Additionally, the dynamics of a spacecraft located at these Lagrange points requires some degree of control so the spacecraft remains in a useful position in cis-lunar space. Current challenges in developing missions for the Earth-Moon system involve modeling the three-body system without solar gravitational effects, solar radiation pressure and atmospheric drag. When modeling this system, it can be expected that computational intensity will become an issue as the number of RSOs considered increases. This would motivate creating a minimally computationally intensive simulation which minimizes the total quantity of RSOs considered but strategically analyzes specific types of orbits based on semi-major axis, eccentricity, and inclination. Creating Lagrange Point based space surveillance network also has inherent limitations such as ranging and observation capabilities. Additionally, such missions may be restricted to minimal maneuvering and plane changes if traditional propellant-based thrusters are utilized due to Δv requirements. Limitations to orbit maneuvers may be mitigated by utilizing other propulsive systems such as electric propulsion and solar radiation sails[14-17]. Alternative orbit maneuvering techniques provide unique opportunities with regards to longer mission life, larger payload due to additional room from lack of propellant; however, these techniques also pose challenges such as the desire to generate quick impulsive thrusts for maneuvers needed in the near-term.

From this work, a contribution will be made in analyzing the physical and operational limitations of a Lagrangian point based surveillance sensor network. A foundational model will be created in MATLAB which simulates space-based surveillance capabilities while also highlighting its limitations. The ground-based SSN capabilities will be analyzed over extended periods of time for satellite constellations of interest. These satellite constellations will encompass diverse orbits profiles whose properties cover a range of orbital elements. For example, specific altitude thresholds will be set for when optical sensors will be employed instead of radar sensors. Additionally, thresholds regarding the apparent magnitude of an object will also be considered. There is an expectation that the behavior of surveillance gaps will be periodic due to nature of orbital motion. This provides some advantages in allowing for the simulation of shorter periods of time. After identifying the current surveillance shortcomings, the space-based surveillance network will be deployed via simulation and its ability to fulfill the shortcomings of the ground-based SSN will be evaluated. All of these aforementioned aspects are found to be the most important qualitative and quantitative indicators which would dictate the necessity and realism of a such a space-based surveillance network.

II. Approach

This project aims to construct a cis-lunar surveillance network by initially understanding the current limitations of existing ground based systems. This leads to the desire to simulate the Earth-Sun-Moon system as well as a more thorough narrow view of the Earth-Moon system and its resident spacecraft. The simulation developed will be utilized to illustrate and analyze the deficiencies that exist in the current ground-based SSN. Additionally, the simulation includes observations made from Lagrange point space-based surveillance sensors. The two-body motion of the Earth-Moon (or Earth-Spacecraft) can be modeled as [18]:

$$\ddot{\vec{r}} = \frac{\mu}{r^2} \frac{\vec{r}}{||\vec{r}||} + \vec{a}_{J_2} \quad (1)$$

The expression above demonstrates that considerations will be given for the acceleration due to J_2 . This acceleration is characterized as:

$$\vec{a}_{J_2} = \frac{-3J_2\mu R_E^2}{2||\vec{r}||^4} \begin{cases} \frac{x}{||\vec{r}||}(1 - \frac{5z^3}{||\vec{r}||^2}) \\ \frac{y}{||\vec{r}||}(1 - \frac{5z^3}{||\vec{r}||^2}) \\ \frac{z}{||\vec{r}||}(3 - \frac{5z^3}{||\vec{r}||^2}) \end{cases} \quad (2)$$

These expressions can be evaluated using ODE45 from MATLAB's Numerical Integration and Differential Equations Library. Building on this gives the orbital position of any spacecraft for which an initial state vector is known. Since this project aims to work with observations it is worthwhile diving in the geometric observation restrictions that exist in the Earth-Sun system. The geometric observational scenario is shown to be:

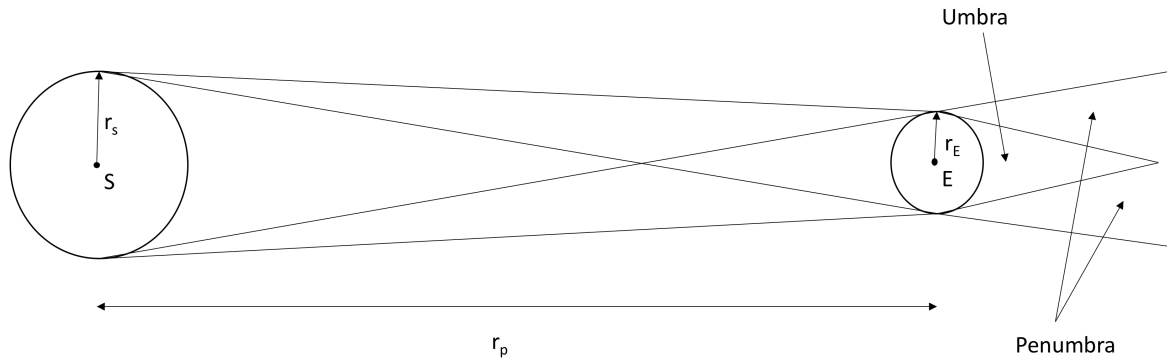


Fig. 1 The geometric setup between the Sun and Earth and the projection of the Umbra behind the Earth.

Fig. 1 shows the eclipse setup between the Sun-Earth system where body S is the Sun and body P is the Earth. The vectors \vec{R}_P is the vector separating the Sun and Earth. The scalar values r_s and r_p are the radius of the Sun and Earth, respectively. The umbra illustrates the region where there is no direct light form the sun while the penumbra is the region where partial sunlight is received. When making optical observations, spacecraft which lie in the penumbra become difficult if not impossible to detect. Thus, this is a region where radar observations would thrive given the RSO of interest is within a radar's functional capabilities.

Observation limitations are also born out of the location and availability of sensors. The SSN is composed of a variety of dedicated, collateral and contributing sensors spread out all over the globe. The location of such sensors is shown in Fig. 2.

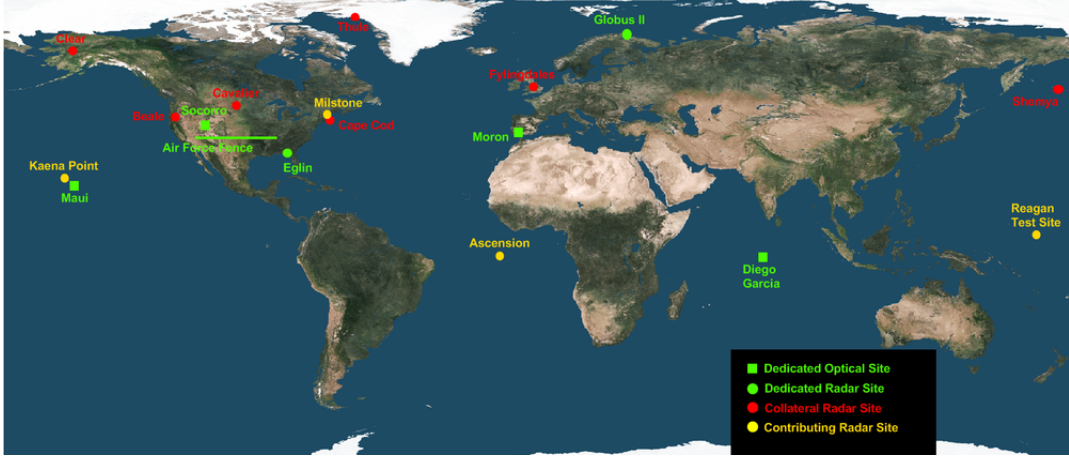


Fig. 2 Location of the Space Surveillance Network Sensors on a Mercator Map. [20]

Each of these sensors was placed strategically to maximize their availability for their intended purposes. For the purpose of this simulation, only the dedicated optical (Maui, Socorro, Moron, Diego Garcia) and radar (Eglin, Globus II) sensors will be included as viable points where line-of-sight (LOS) of an object can be obtained. Integrating an RSO's orbit around the Earth gives their positions relative to the location of the SSN sensors during the Earth's rotation.

We define the angle between the $\vec{\rho}$ (vector between ensor and space object) and \vec{r}_{sensor} as θ . The definition of the dot product can be leveraged to find $\angle(\vec{\rho}, \vec{r}_{sensor}) = \theta$ as:

$$\theta = \cos^{-1}\left(\frac{\vec{\rho} \cdot \vec{r}_{sensor}}{\|\vec{\rho}\| \|\vec{r}_{sensor}\|}\right) \quad (3)$$

The definition of this angle gives a criteria for defining when an object is within the line of sight of a ground-based telescope. A series of criteria have been developed to further indicate a successful LOS sighting for the ground-based SSN. These criteria are outlined in Table 1.

Table 1 Criteria for Detection

Parameter	Criteria	Description
$\ \vec{r}\ $	$\ \vec{r}\ > 15,000 \text{ km}$	Threshold for optical observation
$\ \vec{r}\ $	$\ \vec{r}\ \leq 15,000$	Threshold for radar observation
θ	$\theta < 85^\circ$	Threshold to be in the line of sight
$m_{v,RSO}$	$m_{vSO} < 30$	Threshold for visibility via optical sensor

Additionally, the Earth's shadow provides a 3-D region where detections may not be made due to the Earth's shadow. This criteria is defined mathematically as:

We have $M \subset \mathbb{N}^+$ such that M is the set of all RSOs in orbit. Let $S \subset \mathbb{R}^3$ such that $x, y, z \in S$ where S is the total space where RSOs may reside. Let $\Phi_i = \{\phi_i, \phi_f\}$ where $\phi_i, \phi_f \in \{0, 1\} \forall i \in M$ such that line-of-sight is determined to be true or false. Let $C \subset S$ such that $x_c, y_c, z_c \in C$ such that C contains all the points that live in the umbra. Lastly, we have $L \subset S \forall x_L, y_L, z_L \in L$ such that L contains all the points that reside in sunlit side of the Earth. Thus, for an RSO to be detectable, $x, y, z \in \neg(C \cup L)$.

Making optical detections can prove to be quite complicated; however, a general criteria followed is calculating the apparent magnitude of an object in space. For example, given the apparent magnitude of an object relative to an observer - whether the observer is ground or space-based - provides a threshold to adhere to for considering a detection successful. Coder and Holzinger outline a criteria for computing the apparent magnitude of an object of interest in their

paper about designing Raven class telescopes [21]. Apparent magnitude serves as a common measure of the brightness of an object relative to an observer. The brightness of an object can be a strong indicator of whether or not observations and tracking of an orbiting object can be performed. We can begin by defining the radiometric model to quantify the apparent object of RSOs:

$$m_{s,RSO} = m_{v,\odot} - 2.5 \log_{10} \left[\frac{1}{R^2} \int_{\lambda_{LL}}^{\lambda_{UL}} M_{\oplus}(\lambda) F_r(\theta_I^B, \hat{s}, \hat{R}, \lambda) d\lambda \right] \quad (4)$$

Integrating this equation over the wavelengths of interest and choosing a spherical model gives:

$$m_{v,RSO} = m_{v,\odot} - 2.5 \log_{10} \left[\frac{A\alpha(\rho_{spec}(\psi) + \rho_{diff}(\psi))}{R^2} \right] \quad (5)$$

In [5] we have the area of RSO of interest A , the albedo of the object α , the specular and diffuse components of reflectivity ρ , the solar phase angle ψ and the distance between the observer and the RSO, R . The quantities that need to be computed are defined as:

$$A_{total} = 4\pi r_{sphere}^3 \quad (6)$$

$$\rho_{diff}(\psi) = \frac{2}{3\pi^2} [\sin(\psi) + (\pi - \psi) \cos(\psi)] \quad (7)$$

$$\rho_{spec} = \frac{1}{4\pi} \quad (8)$$

In [6], it becomes evident that the objects apparent magnitudes are computed as if all spheres were spherical and produced Lambertian reflectance. Additionally, the apparent magnitude of the sun is found to be $m_{v,\odot} = -26.73$. While this criteria is designed for one particular sensor and RSO it can be modified so that the apparent magnitude of a sample space can be computed (i.e. cislunar space).

The last important portion of background information comes from the need to understand the CRTBP. During the

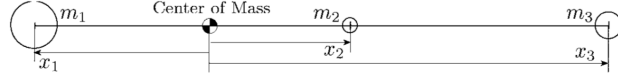


Fig. 3 Co-linear configuration of a three body system where $m_2 \ll m_1, m_3$ [22].

derivation of the CRTBP a series of equations are born [22]:

$$\ddot{x} - \dot{y} = 1 - (1 - \mu^*) \frac{x - x_1}{\rho_1^3} - \mu^* \frac{x - x_2}{\rho_2^3} = \frac{\partial U}{\partial x} \quad (9)$$

$$\ddot{x} + 2\dot{y} = (1 - \frac{1 - \mu^*}{\rho_1^3} - \frac{\mu}{\rho_2^3})y = \frac{\partial U}{\partial y} \quad (10)$$

$$\ddot{x} - \dot{y} = -(\frac{1 - \mu}{\rho_1^3} + \frac{\mu^*}{\rho_2^3})z = \frac{\partial U}{\partial z} \quad (11)$$

In Eq. (9) - (11), the variables ρ and μ are defined as:

$$\rho_i = \sqrt{(x - x_i)^2 + y^2 + z^2} \quad \text{where } i = 1 \text{ or } 2 \quad (12)$$

$$\mu^* = \frac{m_2}{m_1 + m_2} \quad (13)$$

It is worth noting that the subscripts 1 and 2 indicate the body in the CRTBP where $m_1, m_3 \gg m_2$. Additionally, μ^* should not be confused with the gravitational parameter μ since μ^* is merely a mass ratio of the two largest masses in the three-body system. From these equations, the equations for the Lagrange points can be defined as (in numerical

order):

$$L1: x - \frac{1 - \mu^*}{(\mu^* + x)^2} + \frac{\mu^*}{(x - 1 + \mu^*)^2} = 0 \quad (14)$$

$$L2: x - \frac{1 - \mu^*}{(\mu^* + x)^2} - \frac{\mu^*}{(x - 1 + \mu^*)^2} = 0 \quad (15)$$

$$L3: x + \frac{1 - \mu^*}{(\mu^* + x)^2} + \frac{\mu^*}{(x - 1 + \mu^*)^2} = 0 \quad (16)$$

$$L4: x - .5 + \mu^2 = 0 \quad (17)$$

$$L5: x - .5 + \mu^2 = 0 \quad (18)$$

It is worth noting that all of these points are planer. Lagrange points L1 - L3 are co-linear so they do not have a y-component. However, L4 and L5 have y-components defined as:

$$L4: y - \cos(30^\circ) = 0 \quad (19)$$

$$L5: y + \cos(30^\circ) = 0 \quad (20)$$

These equations lead to the following values for the cis-lunar Lagrange Points: It is worth noting that the coordinate

Table 2 Lagrange Points

L - Point	X-Coordinate	Y-Coordinate
L1	0.8491	0
L2	1.1678	0
L3	-0.9929	0
L4	0.5000	0.8660
L5	0.5000	-0.8660

values for the Lagrange Points are computed in non-dimensional terms. In order to get true distances for the cis-lunar space, these values must be multiplied by the average distance between the Earth and Moon. Lastly, it is worth noting that when apparent magnitude is computed for a particular point or object in this simulation each object is taken to be a sphere in order to assume Lambertian reflectance. Each sphere has the properties outlined in Table 3.

Table 3 Spherical Object Properties

Property	Value	Description
r	.10 m	Radius of spherical object
α	.2	Albedo of object

III. Results

The development of the simulation involves the creation of visual representation of line of sight measurements and whether an RSO resides in a currently observable region relative to the sensor. This was implemented as well as a logic which showed where and when a spacecraft was within the line of sight of one of the respective dedicated sensors.

Task I & II : Surveillance Scope Model of Earth-Moon System

Initially, the Sun-Earth-Moon System was modeled for visual purposes. Fig. 4 shows the overarching configuration of the system. The size of the moon is exaggerated in this portion of the simulation for visualization. It is noted that while the Sun is included for demonstration, solar and other planetary effects were not included in this portion or any further portion of the simulation. Next, the umbra shadow for the Earth-Sun-Moon system was modeled and shown

in Fig. 5. In these varying views the red stars are noted placed across the globe. These points indicate the set of ground-based optical and radar observation stations. Each of these sensors is not distinguished by their shape or color in the simulation. However, when either the optical or radar sensors obtain line of sight and the capability observe an RSO the vector drawn from the sensor to is red for optical and blue for radar.

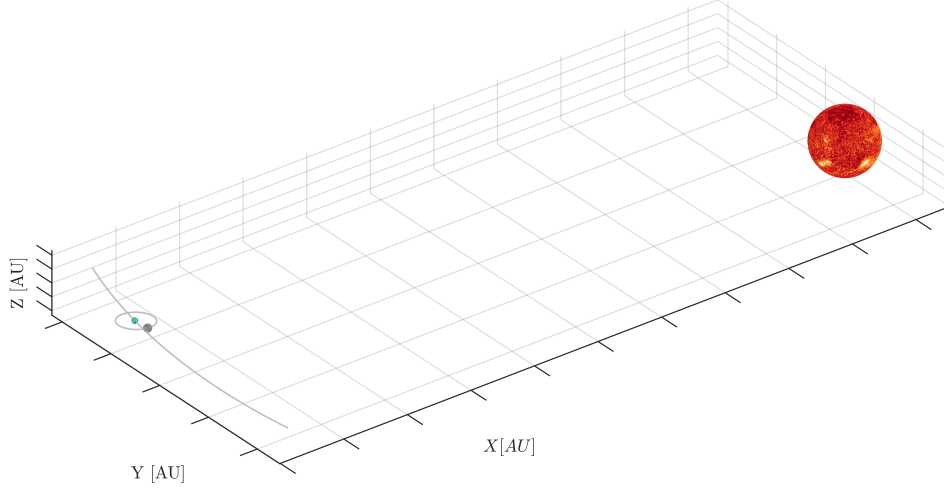


Fig. 4 Sun-Earth-Moon system with orbital track shown for one Lunar period.

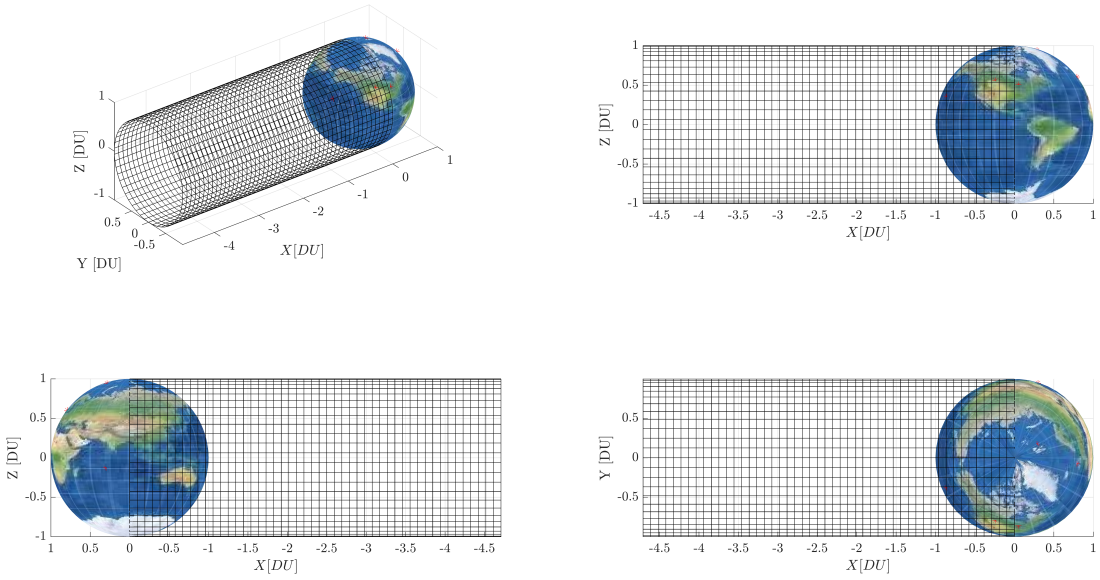


Fig. 5 View of Earth with shadows and sensor locations in Earth canonical units.

Using the criteria defined in Table I, the simulation is run for a subset of the GLONASS constellation (blue) and the ISS (green) using the TLEs from the Celestrak website. The TLEs are converted to initial state vectors for the position

and velocity of each spacecraft. The initial state vector is then entered into MATLAB's ODE45 to propagate the orbit. This leads to obtaining the position and velocity throughout the time period of interest. In the simulation a line between the tracking sensor and the RSO is illustrated to aid in visualizing the operation. Thus, the final simulation illustrates line-of-sight tracking continuously:

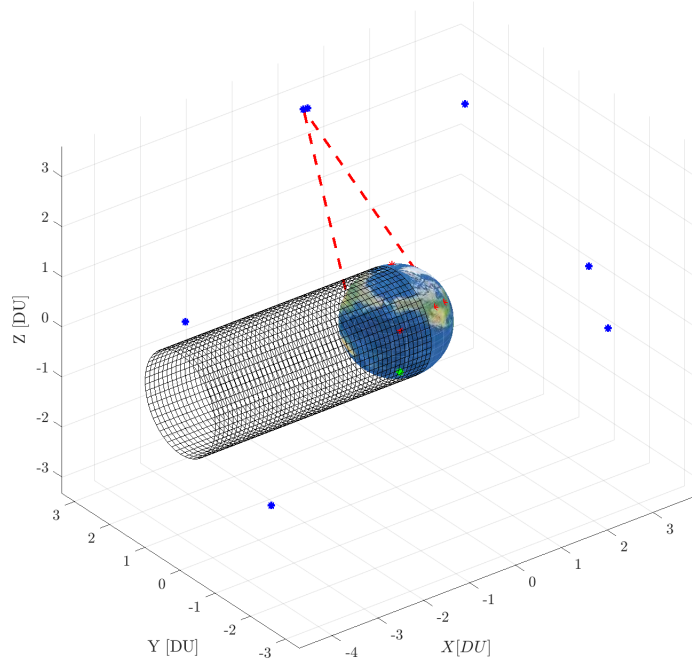


Fig. 6 Line-of-sight tracking simulated for a subset of the GLONASS constellation (blue) and the ISS (green) in Earth Canonical units.

Task III: Current Surveillance Deficiency Determination

The second task of this project sought to assess the current blind spots which exist with ground-based surveillance. It is noted that during the simulation the type of sensor allowed to be utilized to find the line-of-sight of an RSO is narrowed down by the altitude of such RSO. For example, an orbiting object whose altitude is greater than 15,000 km is prioritized for optical sensors. However, an object whose altitude magnitude is less than or equal to 15,000 km is set to have the line-of-sight assessment performed by radar sensors. Of course, from examining Fig. 5 it becomes clear that certain line-of-sight short comings will occur throughout the orbit. Before moving forward with the line-of-sight deficiency analysis, it is also worth noting that sensors are taken to be nominal in their function and observation conditions. In many senses, this is found to be a conservative estimate of the line-of-sight tracking capabilities currently deployed.

For each spacecraft that was propagated the line-of-sight availability was documented as true or false. This was done following criteria established in Table I. The data from all sensors is plotted over the time span leading to instantaneous jumps in whether LOS is true or false. Fig. 7 displays the LOS attained over a 24 hr period for all of spacecraft of interest in this narrow scoped simulation. Fig. 8 contains the same information for radar sensors. Lastly, for optical sensors the apparent magnitude of the RSO becomes an important measurement. Thus, the apparent magnitude of each object relative to each respective sensor of the SSN is plotted in Fig. 9.

The plots show a significant gaps in LOS coverage for the GLONASS constellation and the ISS. Additionally, the LOS of sight condition does not account for anomalous observation conditions. This analysis can be and was extended to several spacecraft constellations using Celestrak TLEs. Their plots have been omitted from this submission due to over cluttering. The general functionality is demonstrated by the Fig. 7-9.

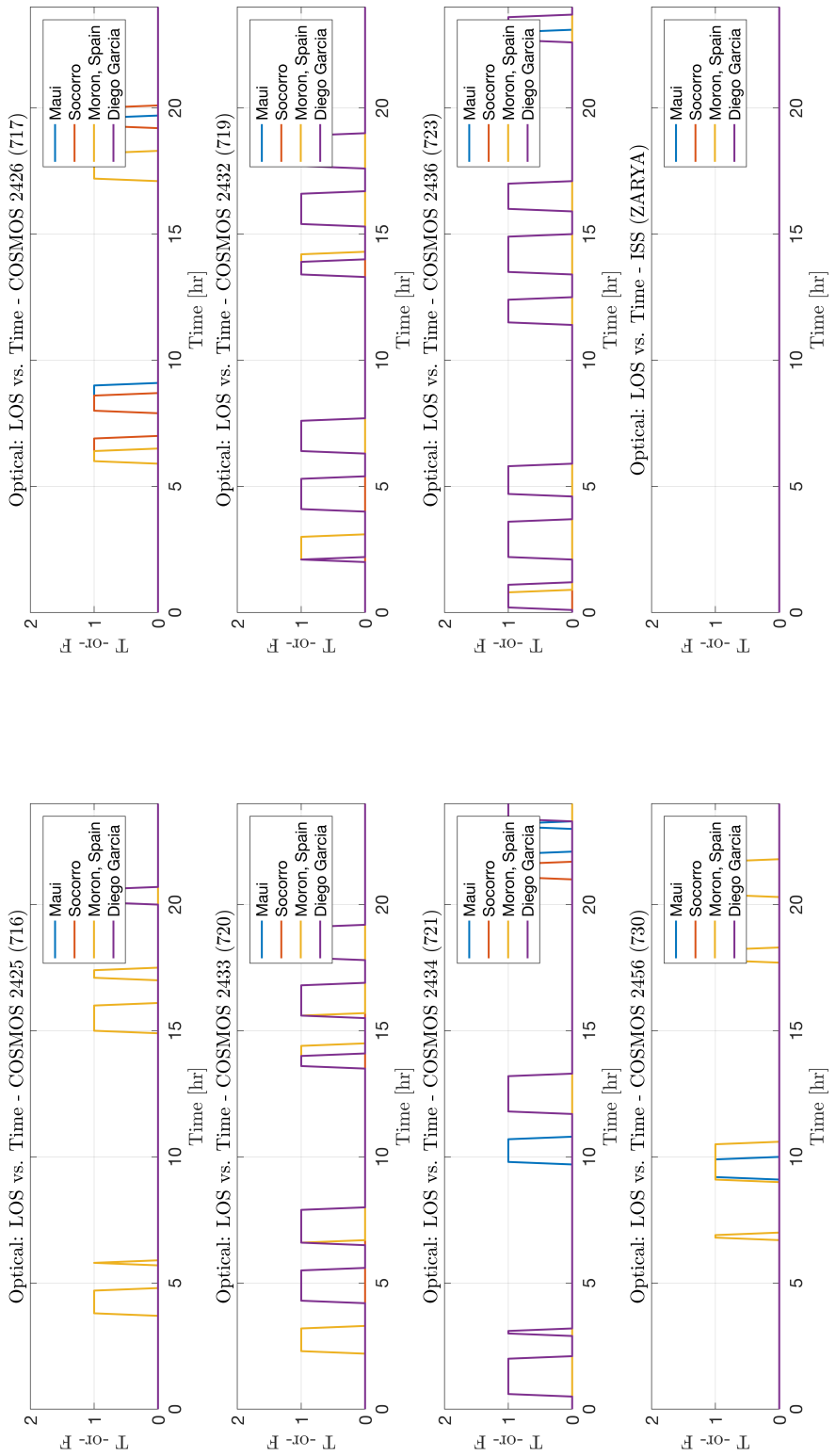


Fig. 7 Optical Line of Sight plots over a 24 hrs period. LOS attainment becomes periodic after an extended period of time. The plot for the ISS shows not LOS attainment because optical sensors are not used at such low altitude per the criteria established in Table I.

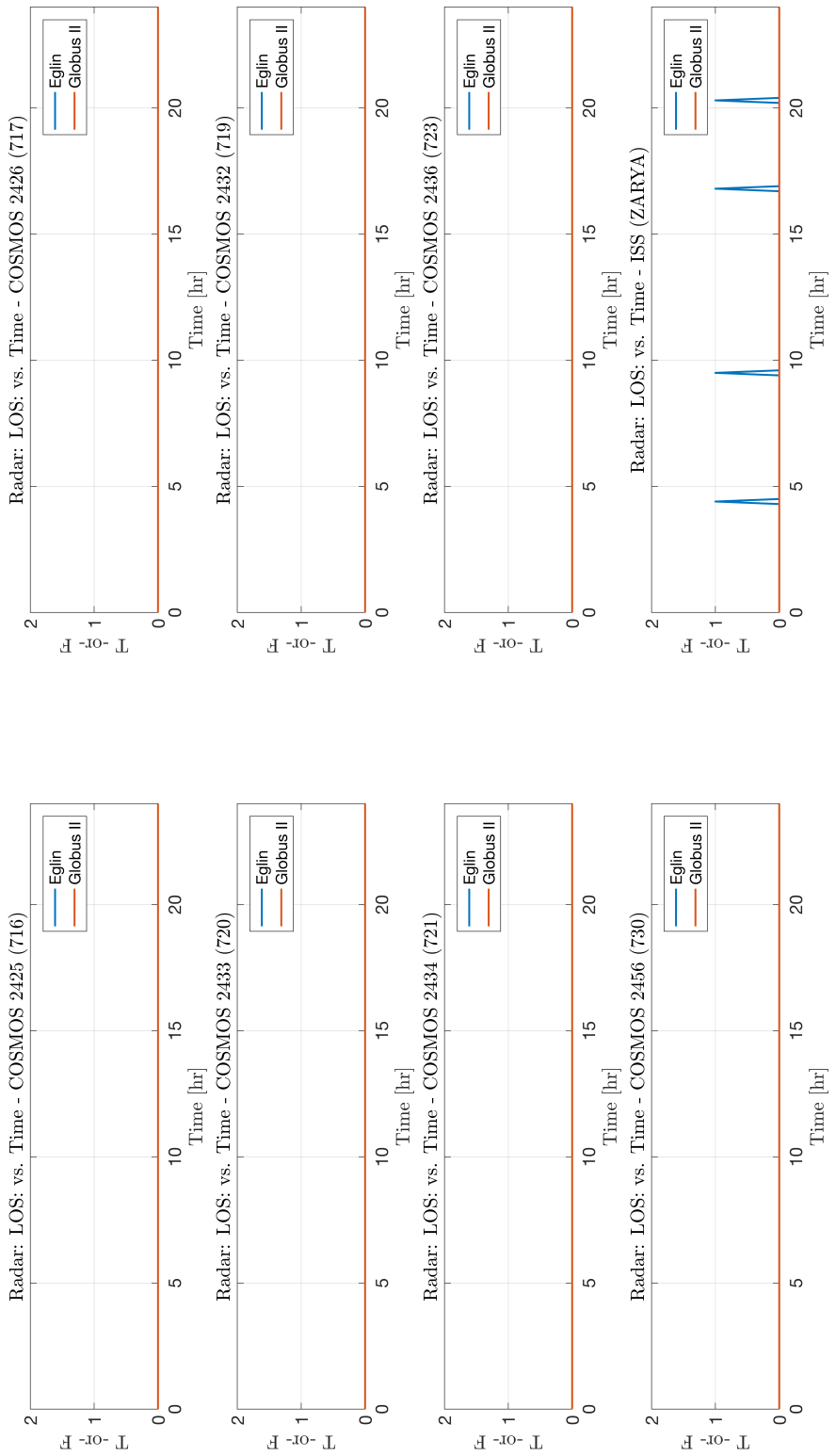


Fig. 8 Radar line of sight attainment for the various spacecraft of interest. It is noted that LOS is attained only for the ISS since radar is meant for lower altitudes per the criteria established in Table I

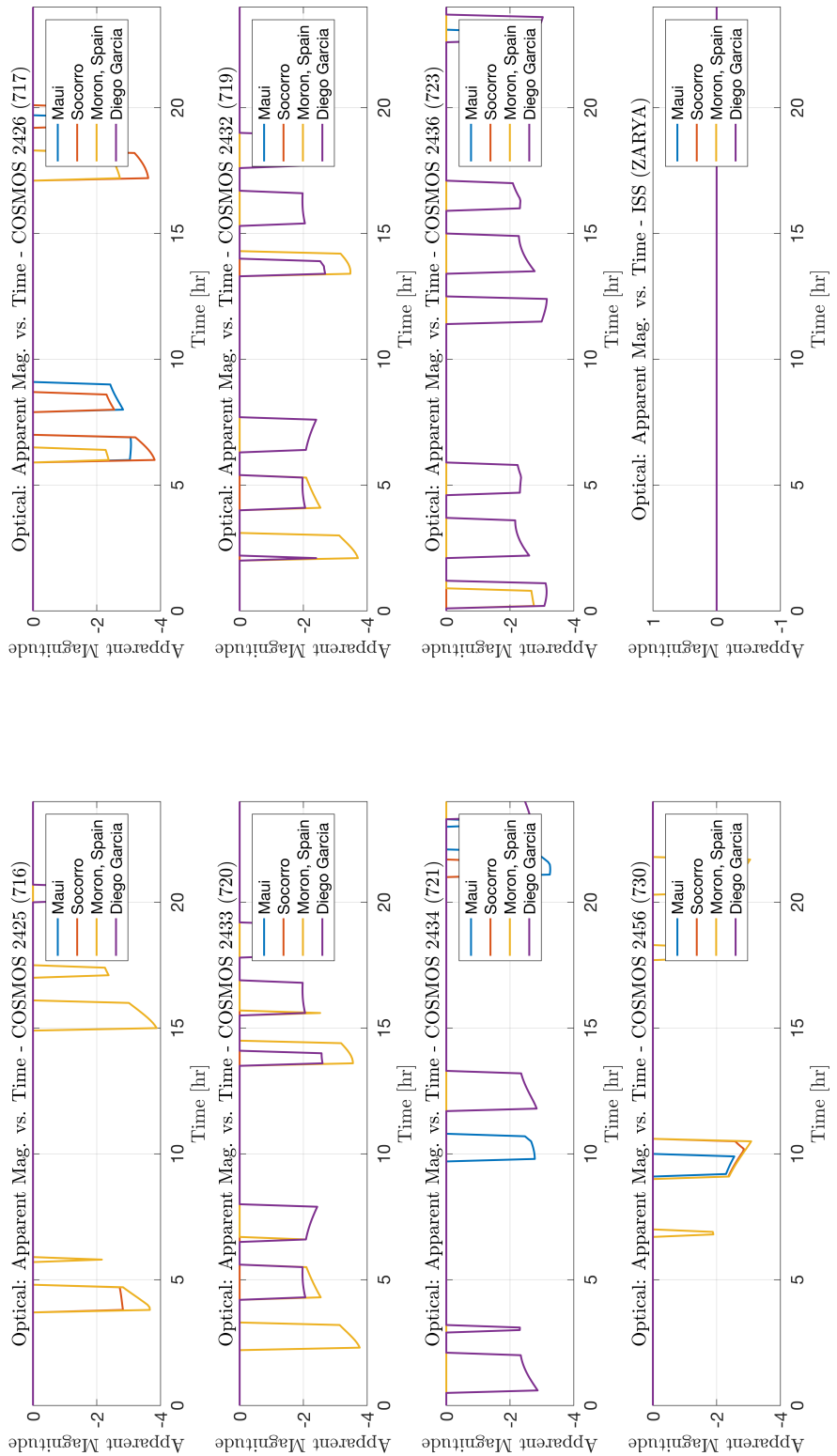


Fig. 9 Apparent magnitude for durations when optical line of sight is obtained. This follows an identical line of sight attainment structure as Fig. 7.

Task IV & V: Surveillance Network Design Configuration & Modeling

A space-based sensor network can prove to be logically complicated and difficult to maintain. For the purposes of this study the space-based sensor network will be located at the 5 Lagrange points in the Earth-Moon. The Lagrange points provide a base where such sensors can reside with minimal maneuvering. In order to evaluate the feasibility of space-based optical sensors, concepts about apparent magnitude and solar phase angle are considered. Thus, for each Lagrange point being considered, the apparent magnitude and the solar phase angle averages and standard deviations are plotted in cis-lunar space. The averages are taken over one lunar period which is about 30 days long. The resulting averages from various vantage points are plotted in Fig. [10] - [19]. From these plots, it is evident that the average apparent magnitudes for an individual sensor based at a particular Lagrange point do not fluctuate significantly. However - as expected through the Lunar period - the solar phase angle has approximately a 180 degree variation. These points are more clearly illustrated in the standard deviation surfaces shown in Fig. [20] - [29]. The standard deviation surfaces in the cis-lunar space show the variation of the values over the Lunar period. These surface plots show less homogeneity between Lagrange points than the average value plots.

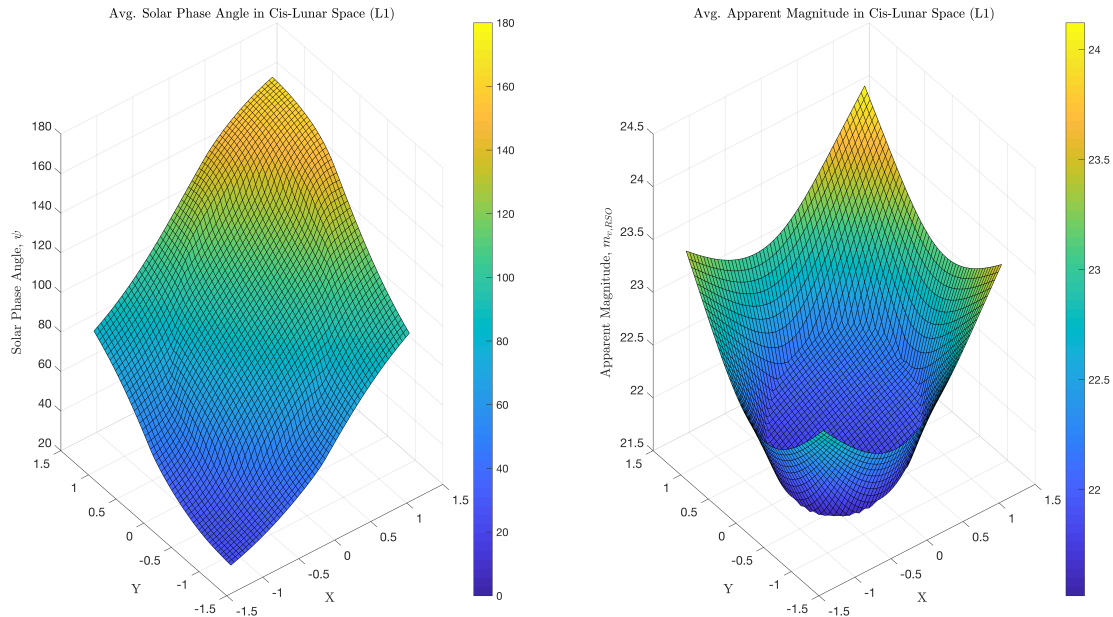


Fig. 10 Isometric view of cis-lunar space with the magnitude of the average solar phase angle (left) and average apparent magnitude (right) across the region demonstrated in a surface plot for a Space-based sensor placed at L1. All distances are normalized by the average distance between the Earth and Moon.